ADVANCED MATERIALS
www.advmat.de

Subcutaneous Administration of a Zwitterionic Chitosan-Based Hydrogel for Controlled Spatiotemporal Release of Monoclonal Antibodies

*Thomas Gréa, Guillaume Jacquot, Arthur Durand, Clélia Mathieu, Adeline Gasser, Chen Zhu, Mainak Banerjee, Elyse Hucteau, Joris Mallard, Pedro Lopez Navarro, Bogdan V. Popescu, Eloise Thomas, David Kryza, Jacqueline Sidi-Boumedine, Giuseppe Ferrauto, Eliana Gianolio, Guillaume Fleith, Jérôme Combet, Susana Brun, Stéphane Erb, Sarah Cianferani, Loïc J. Charbonnière, Lyne Fellmann, Céline Mirjolet, Laurent David, Olivier Tillement, François Lux, Sébastien Harlepp, Xavier Pivot, and Alexandre Detappe**

Subcutaneous (SC) administration of monoclonal antibodies (mAbs) is a proven strategy for improving therapeutic outcomes and patient compliance. The current FDA-/EMA-approved enzymatic approach, utilizing recombinant human hyaluronidase (rHuPH20) to enhance mAbs SC delivery, involves degrading the extracellular matrix's hyaluronate to increase tissue permeability. However, this method lacks tunable release properties, requiring individual optimization for each mAb. Seeking alternatives, physical polysaccharide hydrogels emerge as promising candidates due to their tunable physicochemical and biodegradability features. Unfortunately, none have demonstrated simultaneous biocompatibility, biodegradability, and controlled release properties for large proteins (≥150 kDa) after SC delivery in clinical settings. Here, a novel two-component hydrogel comprising chitosan and chitosan@DOTAGA is introduced that can be seamlessly mixed with sterile mAbs formulations initially designed for intravenous (IV) administration, repurposing them as novel tunable SC formulations. Validated in mice and nonhuman primates (NHPs) with various mAbs, including trastuzumab and rituximab, the hydrogel exhibited biodegradability and biocompatibility features. Pharmacokinetic studies in both species demonstrated tunable controlled release, surpassing the capabilities of rHuPH20, with comparable parameters to the rHuPH20+mAbs formulation. These findings signify the potential for rapid translation to human applications, opening avenues for the clinical development of this novel SC biosimilar formulation.

T. Gréa, A. Durand, O. Tillement, F. Lux
Institut Lumière Matière
UMR 5306
Université Claude Bernard Lyon1-CNRS
University of Lyon
Villeurbanne Cedex 69622, France

T. Gréa, L. David
Université Claude Bernard Lyon 1
INSA Lyon
Jean Monnet University
CNRS, UMR 5223 Ingénierie des Matériaux Polymères (IMP),
Villeurbanne Cedex 69622, France

G. Jacquot, C. Mathieu, A. Gasser, C. Zhu, M. Banerjee, E. Hucteau, J. Mallard, P. Lopez Navarro, B. V. Popescu, S. Harlepp, X. Pivot, A. Detappe
Institute of Cancerology Strasbourg Europe (ICANS)
Strasbourg 67000, France
E-mail: a.detappe@icans.eu

G. Jacquot
Nano-H
St Quentin Fallavier 38070, France

G. Jacquot, C. Mathieu, A. Gasser, C. Zhu, M. Banerjee, P. Lopez Navarro, B. V. Popescu, S. Erb, S. Cianferani, S. Harlepp, X. Pivot, A. Detappe
Strasbourg Drug Discovery and Development Institute (IMS)
Strasbourg 67000, France

The ORCID identification number(s) for the author(s) of this article can be found under https://doi.org/10.1002/adma.202308738

DOI: 10.1002/adma.202308738

1. Introduction

Monoclonal antibodies (mAbs) are widely used in oncology, but their intravenous (IV) administration poses substantial clinical and financial challenges,[1] such as the need for dedicated infusion facilities, aseptic preparation of infusion batches, and difficulties with IV catheter placements.[2,3] To overcome these challenges, subcutaneous (SC) administration was proposed as an attractive alternative technique.[4–6] However, direct SC administration resulted in heterogeneous adsorption because of diffusion of mAbs through the extracellular matrix (ECM), uptake of mAbs by the blood and/or lymphatic capillaries, and presystemic catabolism of mAbs by macrophages.[7,8] The extent to which these factors influence mAbs adsorption, as well as both the rate and extent of mAb adsorption, is affected by the site of SC administration. Moreover, pain at the SC administration site limits clinical tolerability to drug volumes of no more than 1–2 mL and therefore limits the dose of injected mAbs.[9]

To overcome these limitations, recombinant human hyaluronidase, which transiently opens the interstitial space of the SC matrix, was developed to enable the injection of volumes up to 15 mL at a slow flow rate (1.5 to 2 mL min^{-1}).[10,11] The clinical application of SC formulations of trastuzumab and rituximab in combination with rHuPH20 has demonstrated the equivalence of this SC approach to the traditional IV route in terms of therapeutic efficacy and safety with an overwhelming preference from >90% of patients due to its reduced pain and discomfort and improved convenience.[12–14] More recent development of SC formulations of trastuzumab+pertuzumab with rHuPH20[15] confirmed the trend toward applying the SC route of administration despite the signs of immunogenicity observed in ≈20% of patients treated with SC trastuzumab and ≈15% of patients treated with SC rituximab.[16] Nevertheless, SC administration of rHuPh20+mAbs has been limited in terms of administration site the thigh of the patient due to the heterogeneous adsorption observed when SC administration is performed in areas with an abundance of adipose tissue.[7,10] To date, only one enzymatic formulation, rHuPH20 (ENHANZE, Halozyme) has been clinically approved for SC mAb administration, despite the increasing shift from IV-administered biologics toward SC-administered biologics.[17] Consequently, there is a pressing need to explore alternative solutions to the enzymatic approach for SC mAbs administration which may substantially improve patient care management.[17]

As an example of alternative strategy, chemistry-based approaches such as hydrogels have been developed pre-clinically to overcome the limitations of the enzymatic approaches; they offer the possibility of finely controlling the release kinetics of therapeutics ranging from small to large molecules.[18–20] These hydrogels are composed of crosslinked hydrophilic polymer chains within an aqueous environment and exhibit a wide range of adjustable physical and chemical properties.[21–23] A diverse range of naturally sourced and synthetic polymers have been utilized to produce hydrogels through chemical covalent crosslinking.[24,25] Hydrogels have been further tailored to integrate chemically and biologically active recognition moieties such as stimulus-responsive molecules for controlled and sustained drug release properties.[26,27] The hydrogel design facilitates drug release through various mechanisms, such as direct diffusion within the hydrogel matrix, expansion of the network's mesh size due to its swelling properties, or degradation of the hydrogel enabling the release of the drug.[28] However, to date, no hydrogel has successfully been applied in the clinic to provide a controlled release system for large proteins such as mAbs. This can be explained, in part, by their lack of full biodegradability properties after administration and/or their potential lack of complete biocompatibility, which may lead to inflammatory events and/or the difficulty of injecting large volumes without pain to the patient.

A. Durand
MexBrain
13 avenue Albert Einstein, Villeurbanne 69100, France
C. Zhu, M. Banerjee, L. J. Charbonnière, A. Detappe
Equipe de Synthèse Pour l'Analyse
Institut Pluridisciplinaire Hubert Curien (IPHC)
UMR 7178 CNRS/University of Strasbourg
Strasbourg Cedex 2 67087, France
E. Hucteau, J. Mallard
Biomedicine Research Centre of Strasbourg (CRBS)
Mitochondria, oxidative stress
and muscular protection laboratory (UR 3072)
Strasbourg 67000, France
E. Thomas, D. Kryza, J. Sidi-Boumedine
LAGEPP University Claude Bernard Lyon 1
CNRS UMR 5007, Villeurbanne Cedex 69622, France
D. Kryza, J. Sidi-Boumedine
Imthernat Plateform
Hospices Civils of Lyon
Lyon 69002, France
G. Ferrauto, E. Gianolio
Molecular Imaging Center
Department of Molecular Biotechnology and Health Sciences
University of Turin
Turin 10124, Italy
G. Fleith, J. Combet
Université de Strasbourg
CNRS, Institut Charles Sadron (UPR 22)
23 rue du Loess, 67034, Strasbourg Cedex 2 BP 84047, France
S. Brun
Poly-Dtech
Strasbourg 67100, France
S. Erb, S. Cianferani
Laboratoire de Spectrométrie de Masse BioOrganique
IPHC UMR 7178
University of Strasbourg
CNRS, Strasbourg 67087, France
S. Erb, S. Cianferani
Infrastructure Nationale de Protéomique ProFI – FR2048
Strasbourg 67087, France
L. Fellmann
SILABE
Université of Strasbourg
fort Foch, Niederhausbergen 67207, France
C. Mirjolet
Radiation Oncology Department
Preclinical Radiation Therapy and Radiobiology Unit
Centre Georges-François Leclerc
Unicancer, Dijon 21000, France
C. Mirjolet
TIReCS team
INSERM UMR 1231, Dijon 21000, France
F. Lux
University Institute of France (IUF)
Paris 75231, France

To achieve this aim, we selected chitosan to prepare a new type of hydrogels with tunable mAb release properties, as chitosan is known to be biodegradable, biocompatible, comparatively inexpensive, easily chemically modified, and possesses shear-thinning properties as solutions for injectability.[29,30] Here, we report a novel zwitterionic two-component hydrogel composed of chitosan and chitosan@DOTAGA polymers, designed for tunable and controlled SC release of mAbs in mice and non-human primates (NHPs). We demonstrated in mice and in NHPs the biodegradability and biocompatibility of this hydrogel formulation. Furthermore, we validated that the pharmacokinetic characteristics of the hydrogel+mAb formulations were comparable to the clinically-approved rHuPH20 enzymatic approach. Additionally, we extended our investigation by developing multiple SC trastuzumab (anti-ErbB2) biosimilar formulations, showcasing the versatility of this platform as an alternative strategy for SC mAbs delivery. Moreover, in mice, we demonstrated the capability to modulate the release rate of mAbs by adjusting the ratio between chitosan and chitosan@DOTAGA, thereby providing a long-term delivery strategy that is currently unachievable with the enzymatic approach. Overall, our findings highlight the potential of this zwitterionic two-component hydrogel as an innovative and promising system for enhancing the SC administration of mAbs.

2. Results and Discussion

Monoclonal antibody-loading strategy, formulation and characterization of the hydrogel: Chitosan is soluble in acidic aqueous environments due to the protonation of the amine groups of glucosamine residues. Increasing the pH of such solutions above the apparent acid dissociation constants (pKa) of the amine groups results in neutralization and the subsequent formation of a hydrogel, facilitated by hydrogen bonds and hydrophobic interchain interactions if the concentration of the polymer is chosen above a critical value.[31] Within the gelation process of chitosan solutions, the interplay between neutralization and chain disentanglement significantly influences the microstructure and strength of the resultant hydrogels.[32] Furthermore, like in many polyelectrolyte solutions, electrostatic repulsions between chitosan chains can be partially mitigated by increasing the ionic force. This phenomenon enables the formation of gels even at high ionic forces with polyelectrolyte complexes between a polyanion and the chitosan polycation.[33] In light of these aspects, we developed a dual-responsive chitosan-based injectable hydrogel formulation sensitive to both pH and ionic concentration, allowing for controlled release of mAbs.

Synergistic response to both stimuli increases the selectivity of the gelation process to the physiological environment. Specifically, we sought to develop an SC formulation that could be prepared minutes prior to administration to the patient by rapid sterile mixing with an IV-ready mAb formulation. The sterile polymers composed of highly deacetylated (94%) chitosans, one of which was also functionalized by DOTAGA (chitosan@DOTAGA, with a DOTAGA substitution degree of ≈17%), were mixed to form a hydrogel under physiological conditions. In the pH range relevant to this study, DOTAGA is a macrocyclic tetra-carboxylic molecule with protonation constants as follows: $pKa_1 = 1.71$ (H_6L^{2+}/H_5L^{+}), $pKa_2 = 1.88$ (H_5L^{+}/H_4L), $pKa_3 = 4.18$ (H_4L/H_3L^{-}), $pKa_4 = 4.24$ (H_3L^{-}/H_2L^{2-}): $pKa_1 = 9.23$ (H_2L^{2-}/HL^{3-}), and $pKa_2 = 11.08$ (HL^{3-}/L^{4-}).[34] Thus, chitosan@DOTAGA is a zwitterionic derivative with an isoelectric point of 6.9 (i.e., in close proximity to neutral pH) (Figure S1, Supporting Information), likely to form polyelectrolyte complexes with chitosan chain portions baring negative charges. A one-pot process was used to synthesize chitosan@DOTAGA by directly adding DOTAGA anhydride to a hydroalcoholic chitosan solution (see supporting information for synthesis details). The successful amidation between chitosan and DOTAGA anhydride was confirmed by Fourier transform infrared spectroscopy (FT-IR), nuclear magnetic resonance spectroscopy (NMR), and copper titration (see the supporting information for full characterization of the polymer). Chitosan-DOTAGA alone could form a hydrogel after injection of an acidic solution in PBS, acting both on pH and ionic force; however, the stability of this hydrogel in physiological conditions can be improved by the addition of chitosan and the different mass ratio of chitosan@DOTAGA to chitosan (chitosan@DOTAGA:chitosan) to modulate the gelation kinetics as well as the viscoelastic properties of the resulting hydrogel formulation. Thus, we preliminarily selected three chitosan@DOTAGA:chitosan polymer mass ratios (100:0; 67:33; 50:50) to study their impact on the viscosity and injectability of the precursor solutions and the viscoelastic properties of the formulated hydrogels when loaded with mAbs. The structure of the mAb-free hydrogel observed after CO_2 critical drying with scanning electron microscopy (SEM) revealed a fine microstructure with a tightly interconnected network and micron-sized pores with arrangements of porosity at different length scales (**Figure 1A**).

Functionalization of chitosan with DOTAGA and mixing with (unmodified) chitosan led to the rapid formation of a physical hydrogel in physiological conditions at a pH of 7.4 and an ionic force of 300 mOsm L^{-1}. By precomplexing 70% of the grafted polymer's DOTAGA sites with trivalent cations such as gadolinium (Gd^{3+}), no gelation could be observed in these conditions (See supporting information). These results confirmed that the gelation process of this hydrogel is initially driven by polyelectrolyte interactions between negatively charged chitosan@DOTAGA and the positively charged chitosan. We further hypothesized that gelation is initiated through the diffusion of salts, which partially screen the electrostatic interactions and introduce flexibility to the polyelectrolytes, thereby prompting their association into polyelectrolyte complexes (PECs). Subsequently, pH-induced gelation serves as the relay for the initial effect of the salts. When the injectable preparations, formulated in a mild acidic medium at pH 5.5, were placed in PBS to mimic physiological conditions, a pH shift from 5.5 to 7.4 was observed. This shift induced the neutralization of the protonated amine NH_3^+ groups (with pKa ≈6.2), leading to the formation of hydrogen bonds, hydrophobic interactions, and the crystallization of chitosan. As a result, a semicrystalline hydrogel was formed wherein the crystallites act as physical crosslinks with high functionality.[35] After the neutralization of amine groups, the interactions established from PECs still contributed to hydrogel formation, since weaker bonds (H-bonds) are known to form in polysaccharide PECs[36] and serve as secondary interactions to stabilize the interchain nanostructure.

To generate a hydrogel+mAbs formulation, the IV-ready mAbs formulation is minute-mixed with the hydrogel at the desire

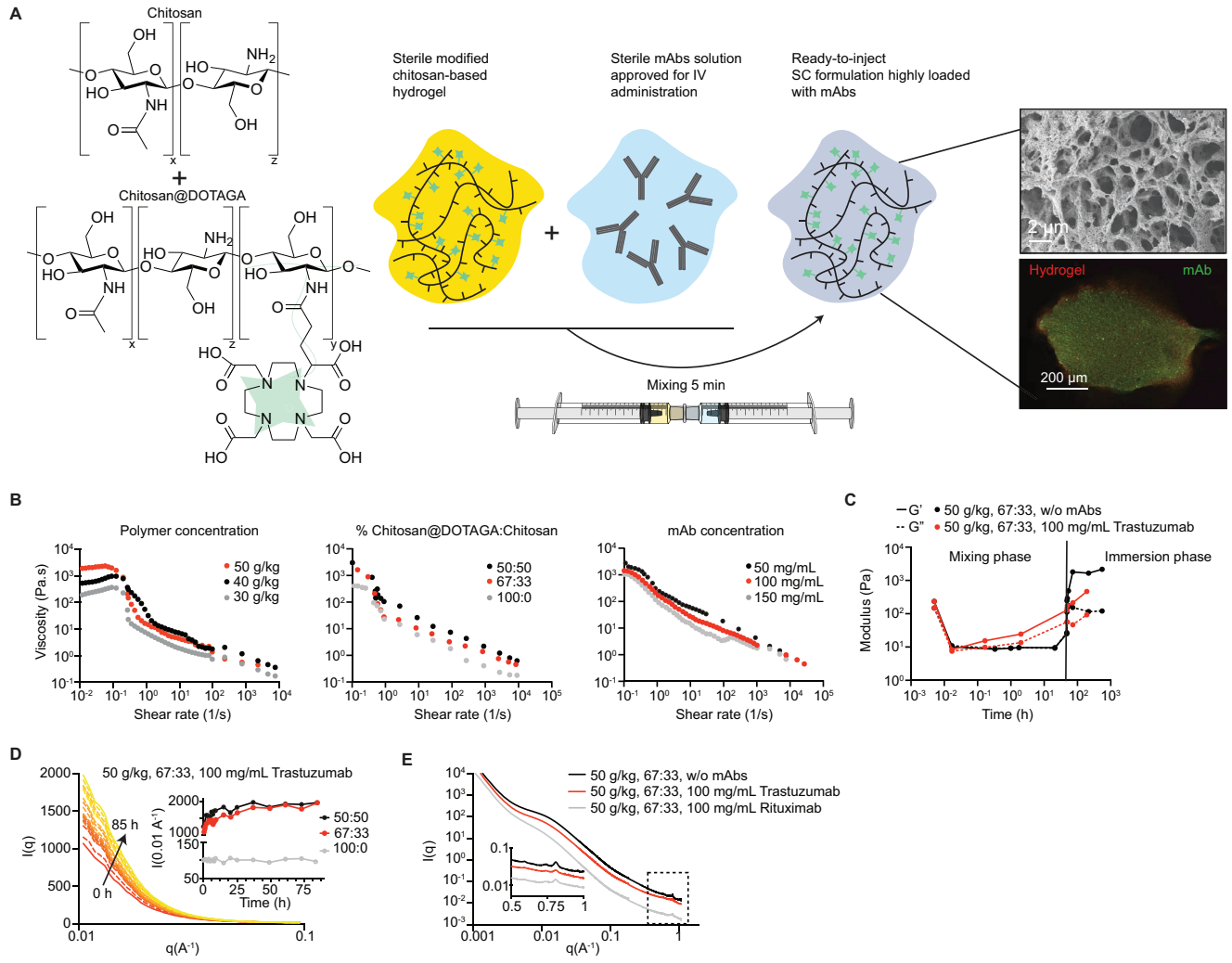

Figure 1. Characterization of the chitosan-based hydrogel formulation. A) Schematic representation of the hydrogel formulation and mixing process for the entrapment of mAbs. Pore sizes of the hydrogel are highlighted by SEM imaging and mAbs homogeneous distribution by confocal imaging. B) Evolution of apparent viscosity with the shear rate reflecting (left) the impact of polymer concentration at a trastuzumab concentration of 100 mg kg^{-1} and a 67:33 chitosan@DOTAGA to chitosan ratio, (middle) the impact of the chitosan composition mass ratio at a total chitosan concentration of 50 g kg^{-1} polymer and a trastuzumab concentration of 100 mg mL^{-1}, and (right) change in the concentration of trastuzumab at a chitosan concentration of 50 g kg^{-1} polymer and a chitosan@DOTAGA to chitosan ratio of 67:33. C) Time evolution of storage (G') and loss (G'') with and without entrapment of trastuzumab (100 mg mL^{-1}) within the hydrogel. D) Dynamics of hydrogel stabilization observed over 85 h by SAXS measurements. Gelation is concomitant with an increase in the scattered intensity in the low-q range. The inset displays a constant structure for the 100:0 hydrogel formulation, which does not form a stable hydrogel over time. E) Evolution of the hydrogel structure at the nanoscale level by SAXS analysis in function of the mAbs loading. Inset represents the diffraction peaks of the hydrated allomorph of chitosan with (020) and (200) diffraction lines.

concentration. As such, we generated various proof-of-concept formulations that were prepared by combining this hydrogel with different FDA/EMA-approved IV-ready mAbs which are already being translated and clinically-approved as SC formulation with the rHuPH20 enzyme in addition to be also available as IV-biosimilars (i.e., trastuzumab, rituximab, and a combination of trastuzumab+pertuzumab) (Figure 1A). Further, we confirmed by physical observation of the hydrogel formation that the polymer solution with 100% chitosan@DOTAGA resulted in a fast-gelling system followed by short-term resolubilization of the formed hydrogel, while the 50% chitosan@DOTAGA and 50% chitosan formulation (50:50 ratio) underwent a very slow gelling process (Figure 1B), resulting in an almost precipitated solid in solution due to continuous disentanglement of the system prior to effective gelation. As a result, the viscosity of the hydrogel was found to be influenced by both the mass ratio of chitosan@DOTAGA:chitosan and the concentration of chitosan used. Specifically, the use of more chitosan@DOTAGA resulted in a lower viscosity, likely due to the tighter conformation of the zwitterionic polymer chains resulting in fewer entanglement knots. Such entanglements are known to impact the properties of a hydrogel when the gelation process is favorable to their preservation.[37] Thus, the initial viscosity of the precursor solution should be related to the mesh size of the hydrogel and its ability to retain the entrapped mAbs.

The formation of the hydrogel at ratios of both 67:33 and 50:50 was not hindered by mAb loading, as evidenced by rheology measurements where the elastic modulus *G'* is higher to the plastic modulus *G''* over a 20-day period. However, the 100% chitosan@DOTAGA formulation (100:0) did not form a stable hydrogel under physiological conditions (Figure 1C). Small angle X-ray scattering (SAXS) allowed to monitor the temporal evolution over the first 85 h post-formulation of the hydrogel formulations with varying ratio of chitosan@DOTAGA to chitosan and with/without entrapment of trastuzumab. The scattered intensity variation demonstrated a structural relaxation of the hydrogel over time (Figure 1D). We observed that the gelation is not instantaneous and mAbs are diffusing out of the chitosan network. Further, replacing trastuzumab by rituximab confirmed the previous results and supposed the versatility of this hydrogel platform to entrap any type of mAbs with reproducible patterns (Figure 1E, Supporting Information).

In vitro identification of the lead candidate formulation: Trastuzumab was chosen as the primary candidate for loading into the hydrogel during its development. This decision was primarily based on the well-defined biotherapeutic activity threshold of this mAb.[38] Consequently, the development process could proceed without the requirement to evaluate the therapeutic activity of trastuzumab after release, provided that there were no modifications to the biologic. As a result, the addition of trastuzumab at 100 mg mL^{-1} led to a thicker and coarser network with larger pores (Figure S2, Supporting Information), while confocal imaging confirmed the homogeneous distribution of trastuzumab within the hydrogel polymer network after fluorescent labeling of both the hydrogel and the mAb (Figure 1A; Figure S3, Supporting Information).

To investigate the impact of the chitosan@DOTAGA:chitosan ratio, we screened the three abovementioned chitosan ratios at a fixed total polymer concentration (50 g kg^{-1}, 5% w/w) and fixed mAb concentration (100 mg mL^{-1} trastuzumab). The release profiles of mAbs were quantified longitudinally by Bradford assay and were consistent with the hydrogel viscosity/viscoelasticity results; the formulation containing 100% chitosan@DOTAGA exhibited the fastest trastuzumab release rate, with 77.5% ± 1.2% of trastuzumab released after 4 h. On the other hand, the 50:50% formulation displayed the slowest in vitro release rate, with 55.5% ± 5.2% of trastuzumab leaked after 4 h. Full release was achieved after seven days for the 100:0 formulation and after ten days for the 67:33 formulation, and ≈80% of the mAb had been released by day 10 for the 50:50 formulation (**Figure 2A**).

Statistically, we observed a significant difference between the 67:33 and 50:50 to 100:0 ratios (*P*-value = 0.04 and 0.03, respectively, Mann-Whitney tests, N = 3). where both formulations allowed the mAb to diffuse from the hydrogel at a slower pace. However, we did not observe a statistical difference between the 67:33 and 50:50 ratios (*P*-value = 0.62, Mann-Whitney tests, N = 3). These findings confirm that the mass ratio of chitosans can tailor the release of the mAbs (67:33 ratio vs 100:0 ratio – *P*-value = 0.04; 50:50 ratio vs 100:0 ratio – *P*-value = 0.03; 67:33 ratio vs 50:50 ratio – *P*-value = 0.62, Mann-Whitney tests, N = 3); an increased proportion of unmodified chitosan leads to slower drug release kinetics.[39] Temperature variations did not influence the release kinetics of the mAbs from the hydrogel, as illustrated by the superimposable curves observed at 20 and 37 °C (Figure S4, Supporting Information).

To evaluate the suitability of the hydrogel formulations for clinical translation, we then evaluated the pressure required to inject these three formulations with a 25G needle designed for SC administration. The pressures required for all three formulations loaded with 100 mg mL^{-1} mAbs were below the clinical pressure threshold of 60 N with such needle[40] (Figure 2B), indicating that these three formulations were potential candidates for further translational applications. However, since the pure chitosan@DOTAGA (100:0 ratio) formulation exhibited a burst release of >50% of mAbs by one hour after formulation and no persistence of a gel over time, this formulation was not considered optimal for further experiments. Rather, we selected the 67:33 formulation as the lead candidate because of its adequate release of the mAbs and because it required a lower force for SC administration than the 50:50 formulation.

The impact of the total polymer concentration at a fixed composition ratio (67:33) and fixed concentration of trastuzumab (100 mg mL^{-1}) resulted in a kinetic release profile dependent of the polymer concentration with 63.6 ± 1.5%, 55.5 ± 5.2% and 58.2%±6.5% of trastuzumab leaked at 24 h post-formulation in phosphate buffer saline (PBS) for the 30, 40, and 50 g kg^{-1} polymer concentration formulation respectively (50 g kg^{-1} vs 40 g kg^{-1} – *P*-value = 0.02; 50 g kg^{-1} vs 30 g kg^{-1} – *P*-value < 0.001; 40 g kg^{-1} vs 30 g kg^{-1} – *P*-value = 0,7, Mann-Whitney tests, N = 3). (Figure 2C). At a fixed polymer concentration (50 g kg^{-1}) and fixed ratio (67:33), the loading of trastuzumab did not impact the release rate with similar kinetic of release (Figure 2D). A similar approach was then performed with various mAbs (rituximab (anti-CD20), bevacizumab (anti-VEGF) and a combination of mAbs (pertuzumab-trastuzumab (both anti-ErbB2) doublets) confirming the observed pattern of mAb release and hence validating the suitability of the hydrogel formulation for the controlled release of various types of mAb (Figure 2E). The above results demonstrate that this straightforward formulation process, which involves sterile mixing of chitosan-based polymer solutions with sterile clinical batches of IV mAbs, can be applied to almost any type and combination of mAbs. Finally, by utilizing the Ritger-Peppas equation[41] (Figure S5, Supporting Information), we determined that the primary mechanism of mAb release from the hydrogel was diffusion. Importantly, we validated that the in vitro release of trastuzumab from the hydrogel did not induce any changes in its physicochemical and biological attributes. This was achieved by comparing the released trastuzumab with reference trastuzumab (trastuzumab IV freshly prepared in PBS). Notably, both samples displayed identical amino acid sequences, primary structures, levels of purity, impurity profiles, charge distributions, total protein concentrations, conformational arrangements, N-glycan configurations, and carbohydrate structures (Figures S6 and S7, Supporting Information).

Preclinical degradation profile, tolerability, and biocompatibility of the hydrogel ± trastuzumab. We then evaluated the capacity of chitosan@DOTAGA-chitosan hydrogels loaded with trastuzumab (hydrogel+trastuzumab) to ensure patient safety by reducing adverse reactions and long-term tissue damage. Achieving these parameters, along with the controlled release properties of the polymer, remains a primary objective for successful

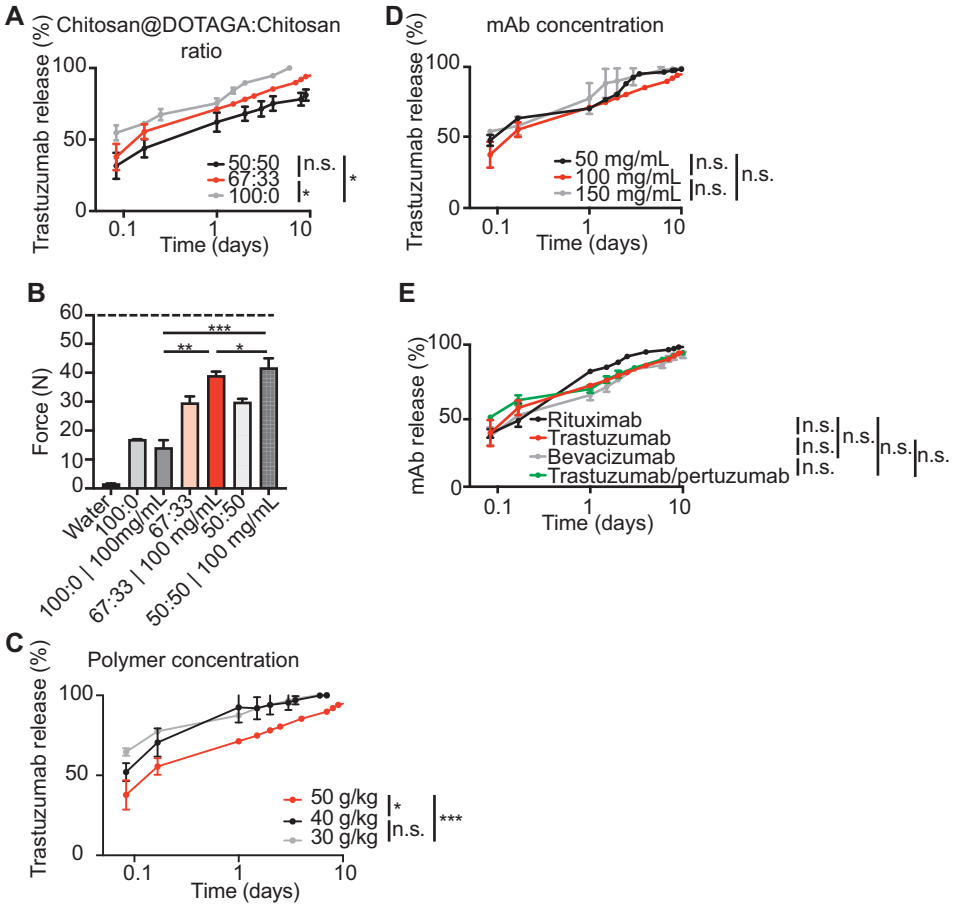

Figure 2. Characterization of the release profiles of the hydrogel formulations. A) Influence of the chitosan@DOTAGA:chitosan ratio on the release of trastuzumab in PBS buffer solution. B) Pressure needed to apply to eject the formulation outside the clinically-used 25 G needle for SC administration. The maximal threshold force of 60 N is highlighted by a dashed line. C) Influence of the total chitosan polymer concentration on the release kinetics of trastuzumab in PBS buffer solution. D) Release rate of trastuzumab from the 67:33 ratio, 50 g kg^{-1} polymer concentration formulation. E) Release kinetics of various monoclonal antibodies or combinations of antibodies routinely used in clinics loaded at 100 mg mL^{-1} from the 67:33 ratio, 50 g kg^{-1} polymer concentration formulation. All the data are represented as mean ± standard deviation and experiments were performed in three biological replicates. *P*-values were calculated using Mann-Whitney tests and are reported as *: $p < 0.05$, **: $p < 0.01$, ***: $p < 0.001$.

translational applications in the field. Hence, the biodegradability and biocompatibility of hydrogel formulations prepared with the 67:33 chitosan@DOTAGA:chitosan ratios were evaluated in vivo in healthy nude mice through SC administration with and without 15 mg of trastuzumab (**Figure** 3A) in 40 or 200 µL injectates (Figure S8, Supporting Information). Longitudinal monitoring of the hydrogel degradation kinetics was achieved using fluorescence imaging of Cy5.5 fluorescent dye-labeled chitosan (Figure 3B), and complete degradation of both the 67:33 hydrogel and the 67:33 hydrogel+trastuzumab at day 27 post-SC administration was confirmed through ex vivo anatomopathological examination of hematoxylin and eosin (H&E) staining (Figure 3C). Interestingly, the kinetic degradation profile remained consistent regardless of the volume injected, exhibiting two distinct regimes: an initial phase with fast degradation of the majority (>90%) of the hydrogel during the first day, followed by a second phase with slow degradation over time until complete degradation was achieved (Figure S8, Supporting Information). The degradation of the hydrogel was further confirmed by inductively coupled plasma-mass spectrometry (ICP–MS) measurements post-labeling of the DOTAGA with Gd^{3+} cations, resulting in a renal clearance and liver degradation of the fragments of the hydrogel (Figure 3D).

Body weight variation in the mice treated with the hydrogel+trastuzumab formulation was demonstrated to be similar to that observed with an FDA/EMA-approved Herceptin SC formulation (Roche – rHuPH20+trastuzumab) (Figure 3E). The low level of proinflammatory cytokines (IL-6, IL-10, TNFα) measured by flow cytometry (Figure S9, Supporting Information) and the low level of expression of Mub40 obtained by immunofluorescence (Figure 3F) confirmed that implantation of the hydrogel+trastuzumab formulation did not cause an adverse inflammatory response in the SC tissue, hence confirming the biocompatibility of these formulations.

Controlled subcutaneous release of trastuzumab from our developed hydrogel in mice. We then investigated the release kinetics of trastuzumab from our developed hydrogel (ratio 67:33, 50 g kg^{-1} of polymer, 100 mg mL^{-1} of trastuzumab), using IVIS imaging (Figure 3G) and compared the pharmacokinetic (PK) profiles, PK parameters, and bioavailabilities (F) to the

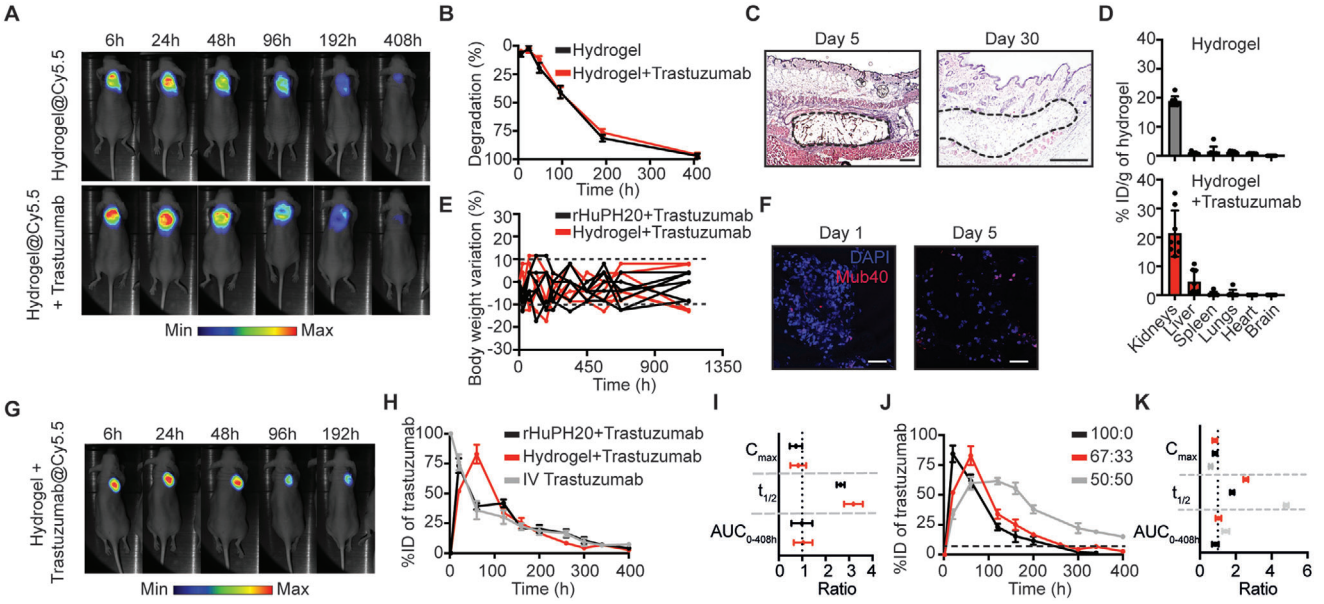

Figure 3. Preclinical evaluation of the hydrogel formulations subcutaneously implanted in mice. A) Representative fluorescence images of the degradation kinetics of the hydrogel and hydrogel+trastuzumab formulation following SC administration of 150 µL of hydrogel and B) quantification of trastuzumab release over time. $N = 6$/group, formulation 67:33, 50 g kg^{-1} polymer concentration, 100 mg mL^{-1} trastuzumab. C) Hematoxylin & eosin (H&E) staining of the SC tissue at day 5 and day 30 post-SC administration of the hydrogel+trastuzumab. Complete degradation of the hydrogel was observed. The dashed line represents the injection site. Scale bar represents 200 µm. D) Biodistribution analysis of the hydrogel and hydrogel+trastuzumab formulation using Gd^{3+}-chelated chitosan@DOTAGA, performed 17 days after SC administration. $N = 8$/group. E) Body weight variation after administration of the hydrogel+trastuzumab formulation (67:33, 50 g kg^{-1} polymer concentration) or the rHuPH20+trastuzumab combination administered with the same trastuzumab concentration (100 mg mL^{-1}). $N = 6$/group. F) Pro-inflammatory immunofluorescence staining (Mub40) of the tissue where the hydrogel+trastuzumab formulation were implanted at days one and five post-SC administration of the hydrogel-trastuzumab confirm the biocompatibility of the formulation in mice. Scale bar represents 50 µm. G) Representative fluorescence imaging of the release kinetics of fluorescent trastuzumab from the hydrogel over time. $N = 9$/group. H) Pharmacokinetic profiles of the hydrogel+trastuzumab, 67:33 ratio; the formulation rHuPH20+trastuzumab; and IV trastuzumab determined by IgG-FLISA. All formulations were administered at 100 mg mL^{-1} trastuzumab. N = 9/group. I) Ratio plot comparing the pharmacokinetic parameters of the hydrogel+trastuzumab formulation and the rHuPH20+trastuzumab formulation to the IV trastuzumab formulation. Data are represented as the mean ± SD. J) Pharmacokinetic profiles of the hydrogel+trastuzumab at different composition ratios. By modifying the mass ratio of chitosan@DOTAGA to chitosan, controlled tunable release of trastuzumab was achieved. The dashed line represents the biotherapeutic activity threshold of trastuzumab. K) Ratio plot comparing the pharmacokinetic parameters of the IV formulation to those of the 3 SC formulations. All the data are represented as mean ± standard deviation.

IV trastuzumab formulation and the commonly employed clinical treatment rHuPH20+trastuzumab. Both SC formulations extended the circulation time of trastuzumab in mice, resulting in half-lives of 121 ± 6 h, 101 ± 2 h, and 38 ± 14 h for the hydrogel, rHuPH20, and IV formulations, respectively, as determined by IgG-fluorescence-linked immunosorbent assay (IgG-FLISA). When normalized to the IV formulation, the half-life was increased by a factor of 3.2 ± 0.2 and 2.6 ± 0.1 for the hydrogel formulation and rHuPH20 formulation, respectively, confirming the sustained release properties of the SC route of administration. Importantly, due to the SC approach, both the hydrogel and rHuPH20 exhibited slightly lower C_{max} values compared to the IV route, with ratios of 0.8 ± 0.1 and 0.7 ± 0.1 for the hydrogel and rHuPH20, respectively. Notably, the hydrogel formulation demonstrated the ability to release trastuzumab with a bioavailability comparable to rHuPH20, without the need to incorporate an enzyme (F = 1.03 ± 0.16 and F = 0.98 ± 0.18) to enhance their release from the SC matrix (Figure 3H,I). These findings confirmed that the hydrogel developed with a 67:33 ratio displayed PK parameters comparable to those of the rHuPH20+trastuzumab formulation, indicating its potential for further clinical translation. Importantly, the PK profile of hydrogel+trastuzumab remained similar regardless of the administration site (neck vs legs) (Figure S10, Supporting Information). Moreover, similar PK properties governed by similar hydrogel degradation kinetics were further confirmed using three additional trastuzumab biosimilars, including Trazimera (Pfizer), SB3 (Samsung Bioepis), and HD201 (PrestigeBiopharma) (Figure S11, Supporting Information), which again showed no significant differences from the results obtained with the rHuPH20+trastuzumab formulation. Furthermore, we observed comparable PK profiles for the hydrogel+rituximab combination and rHuPH20+rituximab (Figure S12, Supporting Information), supporting the versatility of the system.

We further examined the tunability of the hydrogel formulation for modulable temporal release of mAbs by comparing formulations prepared at ratios of 100:0, 67:33, and 50:50 (Figure 3J,K). Our findings confirmed that it is feasible to modify the duration of trastuzumab release on demand by developing either a "softer" hydrogel formulation (100:0 ratio) for short-term release or a more "rigid" hydrogel formulation (50:50 ratio)

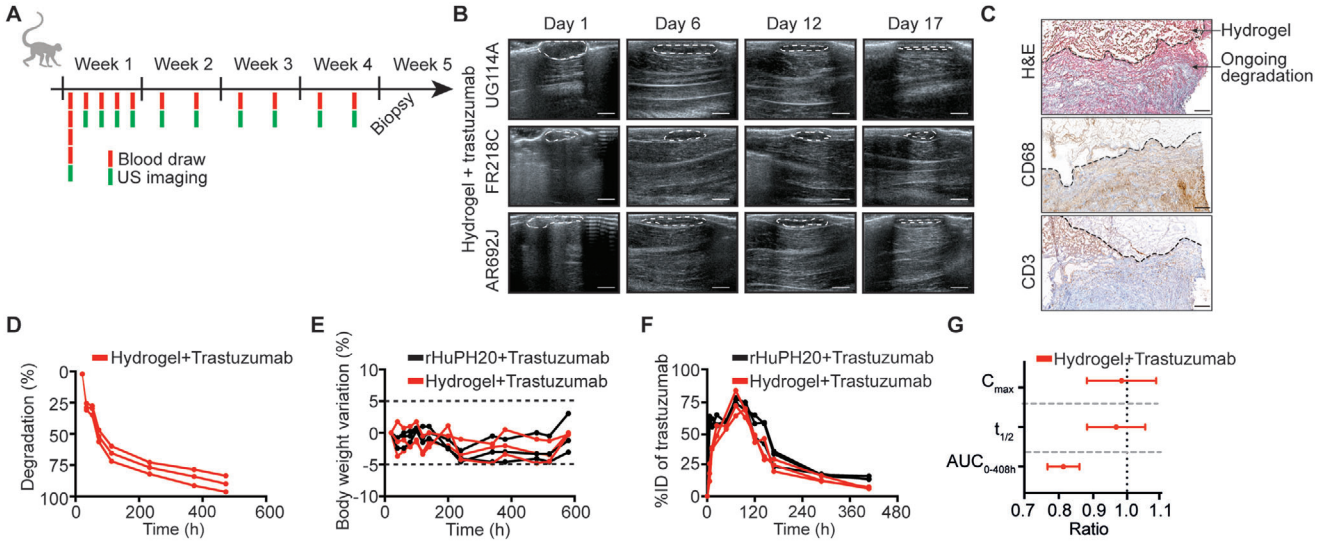

Figure 4. Preclinical validation of the chitosan hydrogel-trastuzumab formulation in nonhuman primates (NHPs). A) Timeline of blood draws and ultrasound (US) imaging performed to monitor the degradation of the hydrogel+trastuzumab formulation SC administered in the leg of NHPs. A total of 1 mL of 100 mg mL^{-1} trastuzumab was administered. B) Representative US imaging depicting the degradation of the hydrogel at the injection site in the 3 NHPs. Scale bar represents 1 cm. C) H&E, CD68, and CD3 immunohistochemistry of the implantation site at day 20 confirming the ongoing process of hydrogel degradation. Scale bar represents 300 µm. D) Degradation profile of the hydrogel based on US imaging. E) Comparison of the change in body weight after SC injection of the hydrogel+trastuzumab formulation in comparison with the rHuPH20+trastuzumab formulation administered at the same trastuzumab concentration (100 mg trastuzumab). F) PK profiles of trastuzumab in plasma based on the hydrogel+trastuzumab and rHuPH20+trastuzumab formulations, determined by HER2-FLISA. G) Ratio plot of the PK parameters of hydrogel+trastuzumab compared to the rHuPH20+trastuzumab formulation. Data are represented as the mean ± standard deviation, $N = 3$ NHPs per group.

for long-term release, suggesting future development to achieve long-term release to allow fewer injections for patients. As a result, the 50:50 ratio hydrogel loaded with trastuzumab led to a sustained release profile that exceeded the threshold for biotherapeutic activity (20 µg mL^{-1} trastuzumab[38]). This sustained release lasted for more than 16 days in murine subjects, with a half-life of 224 ± 6 h. This represents a 4.8 ± 0.1-fold increase compared to the IV route and a 2.2 ± 5.8-fold increase compared to the rHuPH20 formulation (Figure 3J,K). The hydrogel formulation enabled a controlled release lasting twice as long as the rHuPH20 formulation, underscoring the need for further refinement of our formulation to achieve prolonged therapeutic effects. It is worth noting that the modified hydrogel formulations consistently released bioavailable trastuzumab (F = 1 for all 3 evaluated ratios), affirming the suitability of a chitosan-based hydrogel for SC administration of mAbs without compromising their tissue penetration properties. This highlights the potential for advancing the tunability of our formulation for extended therapeutic interventions.

Release profile and biosafety of the hydrogel in nonhuman primates. To apply the degradation kinetics observed in the hydrogel from the mouse study to humans, it was essential to investigate whether the degradation kinetics remained consistent across a range of injection volumes in humans (i.e., 150 µL in mice and up to few mL in human). This evaluation involved studying the degradation kinetics over a specific mL volume range to ascertain their universality and independence from the injection volume. To this end, we SC-administered the formulation prepared at a 67:33 ratio at a volume of 1 mL (containing 100 mg of trastuzumab) in NHPs and monitored the degradation kinetics by ultrasound imaging (**Figure** 4A,B). The observed degradation pattern of the hydrogel was similar to that observed in mice, with an initial rapid degradation followed by gradual degradation until ≈90% of the mass of the hydrogel had disappeared by day 27 post implantation (Figure 4C,D). Following ex vivo immunohistochemistry analysis at the study's conclusion (27 days post implantation), hydrogel fragments persisted within the SC matrix at the injection site as indicated by H&E staining. The presence of immune cells confirmed however ongoing degradation at day 27, supported by remodeling tissues and immune cell activity observed through positive CD68 and CD3 staining (Figure 4C; Figure S13, Supporting Information). Encouragingly, this analysis revealed no evidence of fibrosis, necrosis, cytosteatonecrosis, or lasting damage to the SC area in NHPs following hydrogel-trastuzumab formulation injection. Importantly, despite the presence of residual hydrogel at the terminal study point and ongoing degradation, our formulation exhibited excellent tolerance with no macroscopic nor serological changes, similarly to what is observed with the SC rHuPH20+trastuzumab formulation injected at the same concentration (Figure 4E; Figure S14, Supporting Information). Furthermore, the PK parameters determined by HER2-FLISA of trastuzumab demonstrated similarities, with a half-life of 134 ± 7 h for the hydrogel formulation and 130 ± 11 h for rHuPH20 formulation. The ratio between the hydrogel and rHuPH20 was 0.97 ± 0.13. Additionally, C_{max} values were 74 ± 7% of the injected dose for the hydrogel and 75 ± 2% for rHuPH20, resulting in a ratio of 0.98 ± 0.13. Altogether, this confirms the potential of the hydrogel

platform as a comparable method of administration to rHuPH20 (Figure 4F,G).

3. Conclusion

SC administration of mAbs offers several advantages in clinical routine settings compared to the IV route, including improved patient convenience, compliance, and resource optimization. Here, we present preclinical development of a novel injectable zwitterionic formulation consisting of a functionalized chitosan hydrogel carrier for the tunable and controlled SC release of mAbs. We identified in vitro hydrogel candidates with optimal viscosity, gelation ability, stability, loading capacity, mAb release profiles, and then achieved preclinical biosafety and biodegradation validation of these candidates in both mouse and NHP models. The selected candidate exhibited excellent biocompatibility in both species without causing residual fibrosis or necrosis, which is crucial for future clinical development. Compared to the rHuPH20 enzymatic approach, our hydrogel-trastuzumab formulation achieved a comparable PK profile, validating its potential for clinical application, and matching current outcomes. The zwitterionic nature of our hydrogel may mitigate the limitation of the injection site by interacting with electric charges in the ECM, which can influence the absorption of biologics, leading to the possibility to administer in regions abundant in adipose tissues, known to be less painful for clinical injection. Moreover, by varying the chitosan@DOTAGA:chitosan composition, our hydrogel demonstrated controlled, tunable, and substantially prolonged mAb release, so the hydrogel may offer new clinical prospects such as reduced injection frequency and improved patient convenience.

In conclusion, our findings highlight the clinical potential of our hydrogel formulation for SC mAb delivery. By addressing the unmet medical need for a less expensive and more accessible alternative for the tunable SC administration of mAbs, our advancements hold promise for enhanced patient outcomes and improved clinical practices, presenting opportunities for substantial advancements in patient care.

4. Experimental Section

Preclinical Studies in Mice: All experiments involving animals were reviewed and approved by the Strasbourg University and/or the University of Lyon for Animal Care (A. Detappe – #38306-2022082410083076 and E. Thomas – #43973-2023051711386841). All hydrogel formulations were SC administered with a maximum volume of 150 µL in either the flank or the neck of the animal in accordance with the maximum volume permitted by the committee. IV administration of trastuzumab was performed by tail-vain administration with a final volume of 100 µL.

Preclinical Studies in NHPs: All experiments involving nonhuman primates were approved by the Strasbourg University Committee for Animal Care (L. Felmann – #38464-2022091511095767). The hydrogel+trastuzumab formulation and rHuPH20+trastuzumab were SC administered in the leg of the animal with a maximum volume of 1 mL containing 100 mg of trastuzumab.

Synthesis and Characterization: Details regarding the synthesis and characterization of the hydrogel and a full description of the methods can be found in supporting information.

Statistical Analysis: Data are represented as mean ± standard deviation. All results were analyzed using GraphPad Prism 9.5.1. Statistical analysis was performed using unpaired non-parametric t-test for multiple groups comparison (Mann-Whitney test). Significance was determined at the following cutoff points: $*p < 0.05$, $**p < 0.01$, and $***p < 0.001$.

Supporting Information

Supporting Information is available from the Wiley Online Library or from the author.

Acknowledgements

T.G. and G.J. contributed equally to this Work. A.D. acknowledges support from the Institut de Cancérologie Strasbourg Europe and the European Research Council (ERC) under the European Union's Horizon 2020 research and innovation program (ERC Starting Grant TheranoImmuno, grant agreement No. 950101 and ERC Proof-of-Concept Grant SubNK, grant agreement No. 101138078). This work was also supported by the CNRS, the University of Strasbourg, the Agence National de la Recherche, the French Proteomics Infrastructure (ProFI; ANR-10-INBS-08-03), and the Interdisciplinary Thematic Institute IMS (Institut du Médicament Strasbourg), as part of the ITI 2021–2028 supported by IdEx Unistra (ANR-10-IDEX-0002), the SFRI-STRAT'US project (ANR-20-SFRI-0012), IBiSA and Region Grand Est. The authors are grateful for the use of the X-ray scattering platform DiffériX (ICS, Strasbourg, FRANCE) and the SOLEIL synchrotron (Saint-Aubin, FRANCE) for SAXS-WAXS measurements as well as to the Centre Technologique des Microstructures (CTµ) (Villeurbanne, FRANCE) for their contribution to SEM image acquisition. The authors also thank Dr. Thomas Bizien for his assistance with the SWING beamline, and Dr. Benoit Marteyn for providing access to the Mub40 antibody. Finally, the authors also acknowledge Euro-BioImaging (www.eurobioimaging.eu) for providing access to imaging technologies and services via the Molecular Imaging Italian Node (Torino, Italy).

Conflict of Interest

A.D., O.T., X.P., F.L., T.G., and L.D. are named inventors on a patent application for the hydrogel formulation described in this work. A.D., O.T., and X.P. are co-founders and shareholders of Recobia Therapeutics, which seeks to translate this technology to clinical trials.

Author Contributions

X.P., S.H., F.L., O.T., L.D., C.M., LJ.C., S.C., and A.D. conceived the ideas and designed the experiments. T.G., G.J., A.D., C.M., A.G., C.Z., M.B., E.H., J.M., BV.P., E.T., D.K., J.SB., G.F., E.G., G.F., P.L.N., J.C., S.B., S.E., and L.F. conducted the experiments and analyzed the data. S.H., L.D., O.T., F.L., X.P., and A.D. interpreted the data and wrote the manuscript.

Data Availability Statement

The data that support the findings of this study are available from the corresponding author upon reasonable request.

Keywords

antibody, hydrogel, subcutaneous administration

Received: August 28, 2023
Revised: November 14, 2023
Published online: December 17, 2023

[1] R. S. Epstein, *Clin. Outcomes Res.* **2021**, *13*, 801.
[2] P. Moreau, H. Pylypenko, S. Grosicki, I. Karamanesht, X. Leleu, M. Grishunina, G. Rekhtman, Z. Masliak, T. Robak, A. Shubina, B. Arnulf, M. Kropff, J. Cavet, D.-L. Esseltine, H. Feng, S. Girgis, H. Van De Velde, W. Deraedt, J.-L. Harousseau, *Lancet Oncol.* **2011**, *12*, 431.
[3] M. Villanueva, *Nat. Rev. Clin. Oncol.* **2011**, *8*, 385.
[4] X. Pivot, J. Gligorov, V. Müller, P. Barrett-Lee, S. Verma, A. Knoop, G. Curigliano, V. Semiglazov, G. López-Vivanco, V. Jenkins, N. Scotto, S. Osborne, L. Fallowfield, *Lancet Oncol.* **2013**, *14*, 962.
[5] X. Pivot, J. P. Spano, M. Espie, P. Cottu, C. Jouannaud, V. Pottier, L. Moreau, J. M. Extra, A. Lortholary, P. Rivera, D. Spaeth, H. Attar-Rabia, C. Benkanoun, L. Dima-Martinez, N. Esposito, J. Gligorov, *Eur. J. Cancer* **2017**, *82*, 230.
[6] M. Rummel, T. M. Kim, F. Aversa, W. Brugger, E. Capochiani, C. Plenteda, F. Re, P. Trask, S. Osborne, R. Smith, A. Grigg, *Ann. Oncol.* **2017**, *28*, 836.
[7] L. Kagan, D. E. Mager, *Drug Metab. Dispos.* **2013**, *41*, 248.
[8] P. Zou, F. Wang, J. Wang, Y. Lu, D. Tran, S. K. Seo, *J. Controlled Release* **2021**, *336*, 310.
[9] J. T. Jørgensen, J. Rømsing, M. Rasmussen, J. Møller-Sonnergaard, L. Vang, L. Musaeus, *Ann. Pharmacother.* **1996**, *30*, 729.
[10] L. H. Bookbinder, A. Hofer, M. F. Haller, M. L. Zepeda, G.-A. Keller, J. E. Lim, T. S. Edgington, H. M. Shepard, J. S. Patton, G. I. Frost, *J. Controlled Release* **2006**, *114*, 230.
[11] M. A. Printz, S. S. Dychter, E. P. Denoia, R. Harrigan, B. J. Sugarman, M. Zepeda, J. Souratha, D. W. Kang, D. C. Maneval, *Curr. Ther. Res.* **2020**, *93*, 100604.
[12] C. Jackisch, D. Stroyakovskiy, X. Pivot, J. S. Ahn, B. Melichar, S.-C. Chen, C. Meyenberg, N. Al-Sakaff, D. Heinzmann, R. Hegg, *JAMA Oncol.* **2019**, *5*, e190339.
[13] A. Davies, F. Merli, B. Mihaljevic, N. Siritanaratkul, P. Solal-Céligny, M. Barrett, C. Berge, B. Bittner, A. Boehnke, C. Mcintyre, D. Macdonald, *Lancet Oncol.* **2014**, *15*, 343.
[14] G. Ismael, R. Hegg, S. Muehlbauer, D. Heinzmann, B. Lum, S.-B. Kim, T. Pienkowski, M. Lichinitser, V. Semiglazov, B. Melichar, C. Jackisch, *Lancet Oncol.* **2012**, *13*, 869.
[15] A. R. Tan, S.-A. Im, A. Mattar, R. Colomer, D. Stroyakovskii, Z. Nowecki, M. De Laurentiis, J.-Y. Pierga, K. H. Jung, C. Schem, A. Hogea, T. Badovinac Crnjevic, S. Heeson, M. Shivhare, W. P. Kirschbrown, E. Restuccia, C. Jackisch, *Lancet Oncol.* **2021**, *22*, 85.
[16] N. L. Jarvi, S. V. Balu-Iyer, *BioDrugs* **2021**, *35*, 125.
[17] A. C. Anselmo, Y. Gokarn, S. Mitragotri, *Nat. Rev. Drug Discov.* **2019**, *18*, 19.
[18] J. Li, D. J. Mooney, *Nat. Rev. Mater.* **2016**, *1*, 16071.
[19] J. H. Klich, C. M. Kasse, J. L. Mann, Y. Huang, A. I. D'aquino, A. K. Grosskopf, J. Baillet, G. G. Fuller, E. A. Appel, *Adv. Ther.* **2022**, *6*, 2200102.
[20] S. Correa, E. L. Meany, E. C. Gale, J. H. Klich, O. M. Saouaf, A. T. Mayer, Z. Xiao, C. S. Liong, R. A. Brown, C. L. Maikawa, A. K. Grosskopf, J. L. Mann, J. Idoyaga, E. A. Appel, *Adv. Sci.* **2022**, *9*, 2103677.
[21] Y. Gu, J. Zhao, J. A. Johnson, *Trends Chem.* **2019**, *1*, 318.
[22] Z. Wang, X. Zheng, T. Ouchi, T. B. Kouznetsova, H. K. Beech, S. Av-Ron, T. Matsuda, B. H. Bowser, S. Wang, J. A. Johnson, J. A. Kalow, B. D. Olsen, J. P. Gong, M. Rubinstein, S. L. Craig, *Science* **2021**, *374*, 193.
[23] S. Bernhard, M. W. Tibbitt, *Adv. Drug Delivery Rev.* **2021**, *171*, 240.
[24] S. Correa, A. K. Grosskopf, H. L. Hernandez, D. Chan, A. C. Yu, L. M. Stapleton, E. A. Appel, *Chem. Rev.* **2021**, *121*, 11385.
[25] B. Marco-Dufort, J. Willi, F. Vielba-Gomez, F. Gatti, M. W. Tibbitt, *Biomacromolecules* **2021**, *22*, 146.
[26] B.-H. Shan, F.-G. Wu, *Adv. Mater.* **2023**, https://doi.org/10.1002/adma.202210707.
[27] P. D. Thornton, R. J. Mart, R. V. Ulijn, *Adv. Mater.* **2007**, *19*, 1252.
[28] P. I. Lee, C.-J. Kim, *J. Controlled Release* **1991**, *16*, 229.
[29] S. Peers, A. Montembault, C. Ladavière, *J. Controlled Release* **2020**, *326*, 150.
[30] M. N. V. R. Kumar, R. A. A. Muzzarelli, C. Muzzarelli, H. Sashiwa, A. J. Domb, *Chem. Rev.* **2004**, *104*, 6017.
[31] A. Montembault, C. Viton, A. Domard, *Biomacromolecules* **2005**, *6*, 653.
[32] S. Ladet, L. David, A. Domard, *Nature* **2008**, *452*, 76.
[33] M. Costalat, P. Alcouffe, L. David, T. Delair, *Carbohydr. Polym.* **2015**, *134*, 541.
[34] J. Moreau, E. Guillon, J.-C. Pierrard, J. Rimbault, M. Port, M. Aplincourt, *Chemistry* **2004**, *10*, 5218.
[35] P.-B. Céline, V. Antoine, B. Denis, V. Laurent, D. Laurent, F. Catherine, *J. Appl. Polym. Sci.* **2013**, *128*, 2945.
[36] G. Lalevée, L. David, A. Montembault, K. Blanchard, J. Meadows, S. Malaise, A. Crépet, I. Grillo, I. Morfin, T. Delair, G. Sudre, *Soft Matter* **2017**, *13*, 6594.
[37] S. Ladet, L. David, A. Domard, *Nature* **2008**, *452*, 76.
[38] M. Pegram, S. Hsu, G. Lewis, R. Pietras, M. Beryt, M. Sliwkowski, D. Coombs, D. Baly, F. Kabbinavar, D. Slamon, *Oncogene* **1999**, *18*, 2241.
[39] N. A. Fletcher, L. R. Babcock, E. A. Murray, M. D. Krebs, *Mater. Sci. Eng.: C* **2016**, *59*, 801.
[40] R. P. Watt, H. Khatri, A. R. G. Dibble, *Int. J. Pharm.* **2019**, *554*, 376.
[41] P. L. Ritger, N. A. Peppas, *J. Controlled Release* **1987**, *5*, 37.